





Original Article

ATOX1 Promotes Hepatocellular Carcinoma Carcinogenesis via Activation of the c-Myb/PI3K/AKT Signaling Pathway

Qin Ouyang^{1#}, Siyu Jia^{1,2#}, Qianyu Zhu^{1,3}, Yanmeng Li¹, Huaduan Zi¹, Sisi Chen¹, Pingping He¹, Hengcheng Tang¹, Yanling Li¹, Anjian Xu¹, Bei Zhang¹, Xiaomin Wang⁴, Xiaojuan Ou⁴, Donghu Zhou^{1*}  and Jian Huang^{1*} 

¹Laboratory of Molecular Biology, Beijing Institute of Clinical Medicine, Beijing Friendship Hospital, Capital Medical University, State Key Laboratory of Digestive Health; National Clinical Research Center for Digestive Diseases, Beijing, China; ²Department of Anesthesiology, Peking University People's Hospital, Beijing, China; ³Department of Gastroenterology, Beijing Anzhen Hospital, Capital Medical University, Beijing, China; ⁴Liver Research Center, Beijing Friendship Hospital, Capital Medical University, State Key Laboratory of Digestive Health; National Clinical Research Center for Digestive Diseases, Beijing, China

Received: November 01, 2024 | Revised: May 06, 2025 | Accepted: June 09, 2025 | Published online: July 07, 2025

Abstract

Background and Aims: Despite advancements in diagnostic and therapeutic strategies, hepatocellular carcinoma (HCC) remains a leading cause of cancer-related mortality. Antioxidant-1 (ATOX1) has been implicated in oncogenic processes across various cancer types; however, its specific role in HCC remains unclear. This study aimed to investigate the function of ATOX1 and its underlying molecular mechanisms in HCC. **Methods:** Immunohistochemical analysis was conducted to assess ATOX1 expression in HCC tissues. Cell Counting Kit-8, colony formation, Transwell migration, flow cytometry, and reactive oxygen species (ROS) assays were employed to evaluate the malignant behaviors of tumor cells. A xenograft mouse model was employed to assess the effects of ATOX1 knockdown on tumor growth *in vivo*. DCAC50 treatment was performed to inhibit the copper transport function of ATOX1. RNA sequencing was conducted to explore the potential molecular mechanisms of ATOX1 in HCC. **Results:** ATOX1 expression was significantly elevated in HCC tumor tissues. ATOX1 promoted cell proliferation, colony formation, and migration. Knockdown of ATOX1 suppressed tumor growth *in vivo*. Mechanistically, ATOX1 activated c-Myb, and thus enhanced the malignant phenotype of HCC cells via activation of the PI3K/AKT signaling pathway. Additionally, ATOX1 reduced intracellular copper accumulation and inhibited ROS production and apoptosis. Inhibition of ATOX1 by DCAC50 decreased cell proliferation while increasing ROS levels and apoptosis in HCC cells. Notably, acetylcysteine reversed the reduction in c-Myb expression induced by ATOX1 knockdown. **Conclusions:** ATOX1 may promote HCC carcinogenesis through

the activation of the c-Myb/PI3K/AKT pathway and the inhibition of copper accumulation and oxidative stress.

Citation of this article: Ouyang Q, Jia S, Zhu Q, Li Y, Zi H, Chen S, *et al.* ATOX1 Promotes Hepatocellular Carcinoma Carcinogenesis via Activation of the c-Myb/PI3K/AKT Signaling Pathway. J Clin Transl Hepatol 2025;13(8):630–643. doi: 10.14218/JCTH.2024.00422.

Introduction

Hepatocellular carcinoma (HCC) is the sixth most prevalent and the third most lethal malignancy worldwide.¹ For patients with early-stage or locally advanced HCC, several effective treatment options are available, including radical surgical resection, transarterial chemoembolization, radiotherapy, and molecularly targeted therapies. Nevertheless, HCC is characterized by a propensity for early metastasis and a high recurrence rate, both of which significantly contribute to its poor prognosis.^{2,3} Consequently, a deeper understanding of the molecular mechanisms underlying the occurrence and development of HCC is imperative for improving patient outcomes and developing more effective therapeutic strategies.

Copper, an essential trace element, participates in numerous physiological regulatory processes, including antioxidant defense, energy metabolism, and neurotransmitter synthesis.⁴ An increasing body of evidence suggests that copper and copper-dependent proteins are crucial for cell proliferation, metastasis, and angiogenesis, highlighting their potential as therapeutic targets in cancer.^{5,6} Elevated copper levels have been observed in both tissues and serum of cancer patients, primarily due to the upregulation of copper transporter systems, such as copper transport protein 1, copper chaperone for superoxide dismutase (CCS), and antioxidant-1 (ATOX1).⁷ Furthermore, as a potent oxidant, excess copper elevates reactive oxygen species (ROS) generation and fosters oxidative stress. In cancers, oxidative stress can induce DNA damage and mutations, resulting in genomic instability and the activation of oncogenes.^{8,9}

ATOX1, a copper chaperone protein composed of 68 ami-

Keywords: Antioxidant-1; ATOX1; Hepatocellular carcinoma; Reactive oxygen species; Copper transporting; c-Myb/PI3K/AKT pathway.

#Contributed equally to this work.

*Correspondence to: Jian Huang and Donghu Zhou, Laboratory of Molecular Biology, Beijing Institute of Clinical Medicine, Beijing Friendship Hospital, Capital Medical University, Beijing 100050, China. ORCID: <https://orcid.org/0000-0002-5180-9833> (JH) and <https://orcid.org/0000-0002-9507-5392> (DZ), Tel: +86-10-6313-9310. E-mail: huangj1966@hotmail.com (JH) and donghuzhou@gmail.com (DZ).

no acid residues, facilitates the transfer of copper to ATPases (ATP7A and ATP7B) located on the membranes of the trans-Golgi network and secretory vesicles.¹⁰ In addition to its role in copper homeostasis, ATOX1 acts as an antioxidant, protecting cells from superoxide- and hydrogen peroxide-induced toxicity.¹¹ Recent studies have highlighted the oncogenic role of ATOX1 in various human cancers.^{12–17} ATOX1 is markedly overexpressed in breast cancer, where single-cell tracking studies have shown that it promotes the transfer of copper to ATP7A and lysyl oxidase, enhancing the migratory capacity of breast cancer cells.¹⁷ In non-small cell lung cancer, ATOX1 delivers copper to the nuclear copper-binding protein CRIP2, promoting its ubiquitin-mediated degradation, thereby increasing ROS levels and activating autophagy.¹² Upon copper activation, ATOX1 also functions as a transcription factor, inducing nucleoporin expression and modulating cis-elements of the Cyclin D1 promoter, mediating copper's impact on cell proliferation.¹³ DCAC50, a small-molecule inhibitor, obstructs the copper-binding motif of ATOX1 and CCS, significantly hindering cancer cell proliferation by inducing oxidative stress and reducing intracellular ATP levels.¹⁴ Despite the liver's primary role in copper metabolism, the involvement of ATOX1 in HCC has not been extensively investigated.

In this study, we demonstrated that ATOX1 was significantly overexpressed in HCC tumor tissues compared to adjacent normal tissues. Functional assays confirmed that ATOX1 enhanced HCC cell proliferation and migration, while ATOX1 knockdown suppressed tumor growth *in vivo*. Mechanistically, ATOX1 upregulated c-Myb (also known as MYB) expression and promoted the malignant behavior of HCC cells through activation of the PI3K/AKT signaling pathway. Furthermore, ATOX1 reduced cytoplasmic copper accumulation, decreased ROS generation, and inhibited apoptosis in HCC cells. Inhibition of ATOX1 with DCAC50 similarly suppressed cell proliferation, elevated ROS generation, and promoted apoptosis. In addition, acetylcysteine reversed the reduction in c-Myb expression induced by ATOX1 knockdown. Our findings suggest that ATOX1 may serve as a potential diagnostic biomarker and therapeutic target in HCC.

Methods

HCC patient cohorts and specimens

Fifty pairs of formalin-fixed, paraffin-embedded HCC tissues and adjacent normal liver tissues were obtained from Beijing Friendship Hospital, Capital Medical University. The clinicopathological information is shown in Supplementary Table 1. In addition, frozen HCC tissue samples were used for real-time polymerase chain reaction (PCR) ($n = 6$) and western blot ($n = 3$) analyses. Our study was approved by the Research Ethics Committee of Beijing Friendship Hospital, Capital Medical University, and conducted in accordance with the Declaration of Helsinki. Written informed consent was obtained from all participants prior to enrollment.

Immunohistochemistry (IHC)

Paraffin-embedded tissue sections were dewaxed and hydrated. Antigen retrieval was performed using citrate buffer at pH 6.0. Sections were then blocked with goat serum for 30 min and incubated overnight with a rabbit anti-ATOX1 antibody (dilution 1:200, NOVUS). After washing with PBS, sections were incubated with biotinylated anti-rabbit IgG and subsequently stained using the DAB kit (Zhongshan Golden Bridge Biological Technology, Beijing, China). The staining intensity was assessed by calculating the integrated optical density

under light microscopy using Image-Pro V6.0. The IHC score was calculated by multiplying the staining intensity grade (reflecting high or low ATOX1 expression) by the positive rate score, which represents the percentage of positive areas (0%–50% and 51%–100%).¹⁸ Two experienced pathologists independently assessed the scores.

Cell culture and plasmids

The Huh7, HepG2, and Hep3B cell lines were used in this study. Huh7 cells were obtained from the Cell Bank of the Type Culture Collection of the Chinese Academy of Sciences, Shanghai, China. HepG2 and Hep3B cells were purchased from the Cell Resource Center of the Chinese Academy of Medical Sciences, Beijing, China. HepG2 and Hep3B cells were cultured in Minimum Essential Medium (MEM, Sigma, Germany) supplemented with 10% FBS (Gibco, USA) and maintained in a humidified incubator at 37°C with 5% CO₂. Huh7 cells were cultured in Dulbecco's Modified Eagle's Medium (DMEM, Sigma, Germany) with 10% FBS. A dual inhibitor targeting ATOX1 and CCS (DCAC50, MCE, USA) was dissolved at 10 mM in dimethyl sulfoxide (DMSO, Sigma, USA) and stored at –20°C. It was diluted in the culture medium to a working concentration of 10 μ M.¹⁴ Acetylcysteine, a ROS inhibitor (Selleck, USA), was added to the culture medium at 20 μ M.¹⁹ LY294002 (Abcam), a specific PI3K inhibitor, was used at a final concentration of 20 μ M according to the manufacturer's recommended protocol.²⁰

Full-length ATOX1 genes were amplified by PCR and cloned into the pcDNA3.1-Flag vector (Tsingke Biotechnology, Beijing, China). Vectors were transfected into cells using X-tremeGENE HP DNA transfection reagent (Roche, Basel, Switzerland) following the manufacturer's instructions.²¹ The culture medium was replaced 6 h after transfection. Cells were harvested 24 h post-transfection for qualitative real-time (qRT)-PCR and 48 h for western blot analysis.

RNA interference and Lentivirus transfection

Small interfering RNAs (siRNAs) targeting ATOX1 and c-Myb, along with a control siRNA, were purchased from RiboBio (Guangzhou, China). siRNA transfections were performed using Lipofectamine RNAiMAX reagent (Invitrogen, USA) per the manufacturer's instructions.²¹ The culture medium was replaced 12 h post-transfection.

To generate stable ATOX1 knockdown cell lines, short hairpin RNA (shRNA) targeting ATOX1 was synthesized and ligated into a lentiviral vector tagged with an enhanced green fluorescent protein (OBIO Technology, Shanghai, China). Lentivirus-containing serum-free medium was incubated with cells at 37°C for 12 h, after which the medium was replaced with 10% FBS-containing medium. The transfection efficiency was assessed by qRT-PCR and western blot.

RNA extraction and qRT-PCR analysis

Total RNA was extracted from cells and liver tissues using TRIzol Reagent (Sigma, Germany). One microgram of RNA was utilized for complementary DNA synthesis using the RevertAid™ First Strand cDNA Synthesis Kit (Roche, Switzerland) in a 20- μ L reaction volume. Real-time PCR was performed with SYBR Green PCR Master Mix (Roche, Switzerland) on an ABI 7300 fluorescence quantitative PCR instrument (Applied Biosystems, USA), as previously described.¹⁸ GAPDH served as the internal reference, and each sample was analyzed in triplicate. Relative expression levels were calculated using the 2^{– $\Delta\Delta$ CT} method. Primer sequences used for qRT-PCR are as follows: ATOX1 forward: 5'-GTGCTGAAGCTGCTCTCGG-3', reverse: 5'-GCCAAGGTA

GGAAACAGTCTTT-3'; *c-Myb* forward: 5'-CACAGAACCACACATGCAGC-3', reverse: 5'-CGAGGCGCTTCTTCAGGTA-3'; *GA PDH* forward: 5'-GAGTCAACGGATTGGTCGT-3', reverse: 5'-GACAAGCTTCCCGTTCTCAG-3'.

Western blot analysis

Cells and tumor tissues were lysed on ice for 30 m using a protein lysis buffer containing phosphatase and protease inhibitors (Roche, Switzerland).²¹ Protein concentrations were quantified via the bicinchoninic acid assay. Equal amounts of protein were separated by sodium dodecyl sulfate-polyacrylamide gel electrophoresis (hereinafter referred to as SDS-PAGE) and transferred onto polyvinylidene difluoride membranes (GE, USA). Tricine-SDS-PAGE (ST756, Beyotime Biotechnology, China) was used to separate low molecular weight proteins such as ATOX1 (7 kDa). Membranes were incubated with 5% non-fat milk (Sigma, Germany) in TBST for 1 h, incubated with primary antibodies, and then with horseradish peroxidase-conjugated secondary antibodies (Zhongshan Golden Bridge Biological Technology, Beijing, China). Protein bands were visualized using Image Lab Software (BIO-RAD, USA) with enhanced chemiluminescent protein chromophores (Millipore, USA). All antibodies are listed in Supplementary Table 2.

Cell proliferation and colony formation assays

Cell proliferation was assessed using the Cell Counting Kit-8 (CCK-8) (Yeasen, Shanghai, China) and colony formation assays as previously described.¹⁸ For CCK-8, 4×10^3 cells per well were seeded into 96-well plates, with five replicates per condition. Ten microliters of CCK-8 solution (Yeasen) and 90 μ L of DMEM (Sigma, Germany) with 10% FBS were added per well and incubated at 37°C for 2 h. Absorbance at 450 nm was measured at 0, 24, 48, and 72 h using a label enzyme-labeled instrument (Thermo, USA).

For colony formation, 5×10^3 cells were seeded into six-well plates with daily medium replacement. After two weeks, cells were washed three times with PBS, fixed with 4% paraformaldehyde (Solarbio, Beijing, China) for 30 m at room temperature, and stained with 0.1% crystal violet solution for 10 min.

Cell migration chamber assay

Cell migration assays were conducted using 24-well plates equipped with Transwell inserts (Corning, USA).¹⁸ A total of 2×10^4 cells were resuspended in 200 μ L of serum-free medium and seeded into the upper chamber. The lower chamber was filled with 800 μ L of DMEM containing 10% FBS. After a 24-h incubation, migrated cells were fixed with 4% paraformaldehyde, stained with 0.1% crystal violet, and counted in five randomly selected fields using ImageJ software. Each experiment was conducted in triplicate.

Apoptosis assay

For the apoptosis assay, cells were harvested, washed with PBS, adjusted to a density of 1×10^6 cells/ml, and incubated with Annexin V (BD, USA) at room temperature in the dark for 30 m, following the manufacturer's protocol.²² After an additional 15-m incubation with propidium iodide, the cells were analyzed by flow cytometry to determine apoptotic stages, using FlowJo V10 software for data analysis. The apoptosis rate was calculated to assess the effect of ATOX1 on cell apoptosis.

ROS assay

Intracellular ROS production was examined using the Reac-

tive Oxygen Species Assay Kit (Beyotime, Shanghai, China).²³ Cells were seeded in 96-well plates at a density of 8×10^3 cells per well, with five replicates for each experimental group. A serum-free medium containing the DCFH-DA probe working solution was added to each well and incubated at 37°C for 20 m. Following incubation, cells were washed twice with PBS, and fluorescence intensity was measured using the enzyme-labeled instrument. Meanwhile, cells were seeded in a 96-well plate for the optical density measurement using the CCK-8 assay at 450 nm. ROS levels were quantified by calculating the ratio of the ROS detection value to the CCK-8 value for the corresponding well, according to the manufacturer's instructions.

Inductively coupled plasma mass spectrometry (ICP-MS)

Huh7 cells were incubated in complete DMEM supplemented with 100 μ M copper for 24 h. Subsequently, the medium was replaced with a copper-free medium, and cells were incubated for an additional 24 h. Following incubation, cells were trypsinized and washed twice with PBS. Samples were harvested and digested using a mixture of nitric and perchloric acids and diluted with ultrapure water.¹⁵ The copper content was quantified using ICP-MS (iCAP 7400, Thermo, Waltham, MA, USA).

Immunoprecipitation (IP)

HCC cells overexpressing ATOX1 and *c-Myb* were lysed in IP lysis buffer for 30 m. A total of 500 μ g of protein was mixed with 30 μ L of pre-treated protein A/G beads (Selleck, USA) and incubated overnight at 4°C. Subsequently, 4 μ g of primary antibody was added and rotated at 4°C for 4 h. The beads were then collected and washed three times with IP binding buffer. A 2 \times loading buffer was added, and the mixture was boiled for 5 m. The supernatant was analyzed by western blotting.²⁴

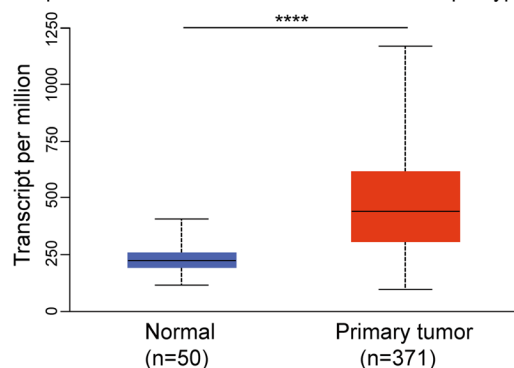
RNA sequencing

Total RNA was isolated from Huh7 cells with either overexpression or knockdown of ATOX1 using TRIzol reagent (Invitrogen, USA). RNA sequencing was performed as previously described.¹⁸ Differentially expressed genes (DEGs) in treated Huh7 cells were identified using the Student's t-test. Cutoff criteria for significant differential expression were $|\log_2 \text{fold change}| \geq 1$ and $q < 0.05$. Statistical significance was further assessed using Fisher's exact test followed by Benjamini correction. An adjusted *p*-value < 0.05 was considered statistically significant.

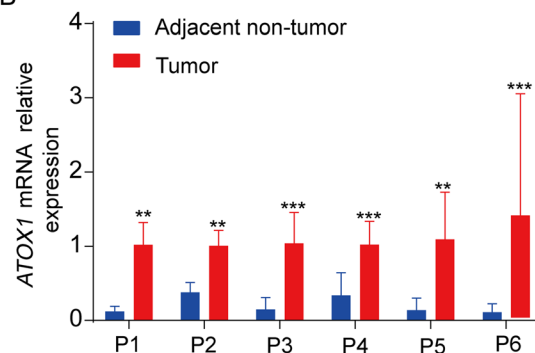
Xenograft mouse models

Twenty four-week-old female BALB/c nude mice were obtained from Vital River Laboratory Animal Technology Company (Beijing, China) and maintained in a sterile environment under the approval of the Animal Experiments and Experimental Animal Welfare Committee of Capital Medical University, as previously described.¹⁸ All procedures followed the Guidelines of Capital Medical University for Animal Experiments and the Experimental Animals Management Committee. In brief, mice were randomized into two groups ($n = 10$) and subcutaneously injected with Hep3B^{sh-NC} or Hep3B^{sh-ATOX1} cells, each suspended in 200 μ L of a 1:1 mixture of Matrigel (BD Biosciences, USA) and PBS. After four weeks, mice were euthanized, and xenograft tumors were excised for immunohistochemical analysis. Tumor size and weight were measured, and tumor volume was calculated using the formula:

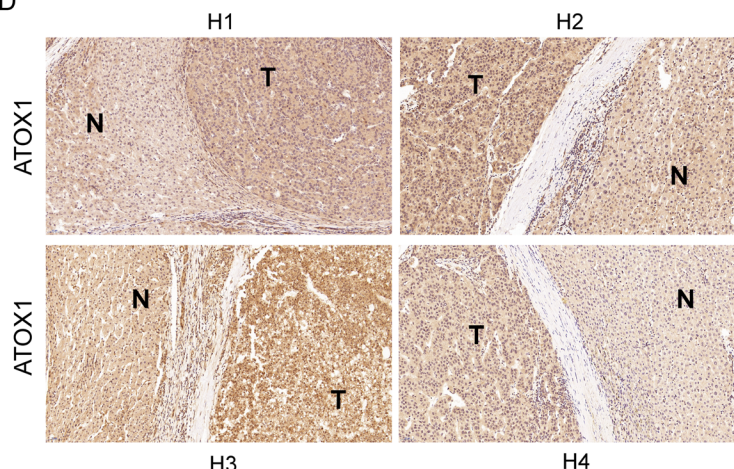
A Expression of ATOX1 in LIHC based on sample types



B



D



C

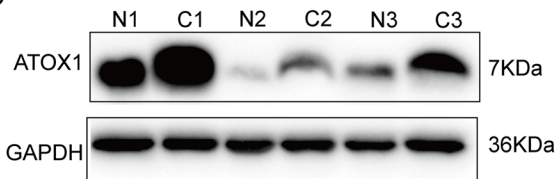


Fig. 1. Expression profile of ATOX1 in HCC. (A) Analysis of ATOX1 transcripts in HCC tissues and adjacent normal tissues was conducted using the TCGA-LIHC database. (B) The mRNA expression of ATOX1 was analyzed in six pairs of HCC and adjacent normal tissues. (C) The protein expression levels of ATOX1 were assessed in three pairs of HCC and adjacent normal tissues ('N' represents adjacent normal tissue and 'C' represents HCC tissue). (D) ATOX1 expression in tumor tissues from 50 HCC patients was analyzed by IHC staining, with images from four representative patients presented ('N' represents adjacent normal tissue and 'T' represents tumor tissue); scale bar, 100 μ m; magnification, $\times 20$. ** p < 0.01, *** p < 0.001, and **** p < 0.0001. HCC, hepatocellular carcinoma; LIHC, liver hepatocellular carcinoma; TCGA, The Cancer Genome Atlas; IHC, immunohistochemistry; ATOX1, antioxidant-1.

$$\text{Volume} = \frac{\text{length} \times \text{width}^2}{2}.$$

Data are presented as means \pm standard deviations. A p -value < 0.05 was considered statistically significant.

Statistical analysis

Bioinformatic analyses were performed using R, command-line interfaces, and online bioinformatics tools. Data from The Cancer Genome Atlas (TCGA), accessed via the UALCAN website (<https://ualcan.path.uab.edu/>), were employed to evaluate ATOX1 expression in HCC tumors versus adjacent normal tissues and to explore correlations between ATOX1 expression, TNM stage, and patient survival. KEGG pathway enrichment analysis was performed on DEGs to investigate gene expression changes. Gene Set Enrichment Analysis was performed to identify pathways differentially enriched between control and ATOX1 knockdown groups. Protein-protein interaction networks of DEGs were analyzed using STRING (<https://cn.string-db.org>) and functionally categorized.

All statistical analyses were conducted using GraphPad Prism 9.0 software (GraphPad Software Inc., USA). Group differences were analyzed using the Student's t -test or one-way ANOVA. The chi-square test was used to analyze the distribution and correlation of categorical variables. All experiments were performed in triplicate unless otherwise noted.

Results

ATOX1 expression was upregulated in HCC tumor tissues compared with adjacent normal tissues

ATOX1 expression in HCC and adjacent noncancerous tissues was examined using the TCGA-LIHC dataset accessed via the UALCAN website. These data showed that ATOX1 transcript levels were higher in HCC samples compared to adjacent noncancerous tissues (Fig. 1A). To further validate these findings, qRT-PCR ($n = 6$) and western blot analysis ($n = 3$) were performed on HCC tissues and matched non-tumor tissues obtained from Beijing Friendship Hospital, Capital Medical University. The results demonstrated that both ATOX1 mRNA and protein levels were markedly higher in HCC tumors than in adjacent normal tissues (Fig. 1B and C). Additionally, IHC staining was performed to assess ATOX1 expression in tumors and adjacent normal tissues from 50 HCC patients, revealing a significant increase in ATOX1 expression in HCC (Fig. 1D). However, in the current study, no correlation was observed between ATOX1

expression levels and tumor size, Edmondson–Steiner grade, serum AFP level, or TNM stage (Supplementary Table 1). Analysis of the TCGA-LIHC dataset also revealed no statistically significant association between ATOX1 expression and TNM staging or survival prognosis in HCC (Supplementary Fig. 1A and B).

ATOX1 promoted proliferation, colony formation, and migration of HCC cells

To elucidate the role of ATOX1 overexpression in the proliferation and migration of HCC cells, we engineered Huh7 and HepG2 cell lines to overexpress ATOX1. The successful overexpression was confirmed by Western blot and qRT-PCR (Fig. 2A, Supplementary Fig. 2A). Functional assays demonstrated that ATOX1 significantly enhanced proliferation, colony formation, and migration of HCC cells (Fig. 2B–D). Moreover, ATOX1 overexpression decreased E-cadherin protein levels (Fig. 2E).

Subsequently, we employed siRNA targeting ATOX1 to downregulate its expression in Huh7 and HepG2 cells (Fig. 3A, Supplementary Fig. 2B). The silencing of ATOX1 markedly inhibited proliferation and colony-forming capacity (Fig. 3B and C). Furthermore, Transwell assays indicated a reduction in migrating cells following ATOX1 knockdown (Fig. 3D), accompanied by increased E-cadherin and decreased N-cadherin expression (Fig. 3E). Collectively, these results suggested that ATOX1 plays a pivotal role in promoting proliferation and migration of HCC cells.

ATOX1 knockdown inhibited tumor growth *in vivo*

To investigate the effect of ATOX1 on tumor growth *in vivo*, we established Hep3B cell lines with stable ATOX1 knockdown (Supplementary Fig. 3A and B) and performed subcutaneous injections of Hep3B^{sh-ATOX1} and Hep3B^{sh-NC} cells into nude mice. Tumor growth was monitored, and tumors were harvested four weeks post-injection. IHC staining confirmed ATOX1 downregulation in the Hep3B^{sh-ATOX1} group (Supplementary Fig. 3C). Notably, both tumor volume and weight were significantly diminished in the Hep3B^{sh-ATOX1} group compared to the Hep3B^{sh-NC} group (Fig. 3F). These results demonstrated that ATOX1 knockdown remarkably inhibited tumor growth *in vivo*, corroborating its suppressive effect on HCC growth.

ATOX1 facilitated proliferation and migration of HCC cells by activating the PI3K/AKT signaling pathway

To investigate ATOX1's influence on HCC-related pathways, RNA-sequencing was performed on ATOX1-overexpressing and ATOX1-silenced Huh7 cells. DEGs were visualized via volcano plots (Supplementary Fig. 4A and B). KEGG pathway analysis identified significantly enriched biological pathways in each group, prominently highlighting the PI3K/AKT pathway (Fig. 4A, Supplementary Fig. 4C). Additional relevant pathways were identified through Gene Set Enrichment Analysis of DEGs in the ATOX1 knockdown group (Supplementary Fig. 4D). These results suggested that ATOX1's oncogenic effects in HCC cells might be mediated through the activation of the PI3K/AKT pathway.

The PI3K/AKT pathway is a well-established signaling cascade implicated in HCC tumorigenesis and progression, critically regulating cell proliferation, oxidative stress, and apoptosis.^{25,26} We investigated ATOX1's role in modulating this pathway. ATOX1 knockdown suppressed phosphorylation of AKT and mTOR in Huh7 and HepG2 cells, whereas ATOX1 overexpression promoted their phosphorylation (Fig. 4B). To further elucidate whether ATOX1 exerts pro-oncogenic effects

via the PI3K/AKT pathway, rescue experiments were conducted using LY294002, a PI3K inhibitor. Western blot analysis revealed that LY294002 attenuated ATOX1-induced activation of AKT/mTOR signaling (Fig. 4C and D). Moreover, LY294002 diminished the ATOX1 overexpression-induced enhancement of cell proliferation and migration (Fig. 4E–G). These results suggested that ATOX1 promoted oncogenic effects in HCC cells through activation of the PI3K/AKT signaling pathway.

ATOX1 might activate the PI3K/AKT signaling pathway by upregulating c-Myb

To elucidate the mechanism by which ATOX1 modulates the PI3K/AKT signaling pathway, we examined 13 hub genes in the ATOX1 knockdown group and 14 genes in the ATOX1 overexpression group, all intricately associated with the PI3K/AKT signaling pathway (Fig. 5A and B). Protein-protein interaction network analysis of these pathway-related genes revealed a connection between ATOX1 and c-Myb/PI3K/AKT (Fig. 5C, Supplementary Fig. 5). Recent studies have implicated c-Myb in cancer cell proliferation, invasion, and apoptosis through regulation of signaling pathways, including PI3K/AKT.^{27–29} Consistent with the RNA-sequencing data, ATOX1 knockdown decreased c-Myb expression, whereas ATOX1 overexpression elevated c-Myb levels (Fig. 5D–G). Although IP results indicated no direct interaction between ATOX1 and c-Myb (data not shown), western blot analysis revealed that c-Myb knockdown attenuated ATOX1-mediated activation of the AKT/mTOR pathway (Fig. 5G). Conversely, c-Myb overexpression counteracted the inhibitory effect of ATOX1 knockdown on AKT and mTOR phosphorylation (Supplementary Fig. 6). These findings suggested that ATOX1 may activate the PI3K/AKT pathway by upregulating c-Myb.

ATOX1 decreased copper accumulation and inhibited cellular ROS levels and apoptosis in HCC cells

Given ATOX1's pivotal role in copper secretion and transport, we hypothesized that its pro-carcinogenic effects might be associated with its copper transport function. First, total copper content was quantified in Huh7 cells treated with the culture medium containing 100 μ M CuSO₄ using ICP-MS. The results showed a significant reduction in total copper content in ATOX1-overexpressing Huh7 cells (Fig. 6A). Next, ROS levels were measured using a ROS assay. ATOX1 overexpression decreased ROS levels, whereas silencing ATOX1 caused a marked increase in ROS (Fig. 6B and C). Excessive ROS generation induced oxidative stress, potentially leading to apoptosis or other forms of cell death. Western blot analysis showed decreased expression of apoptosis-related proteins BAX, cleaved Caspase-3, and cleaved Caspase-9, alongside upregulation of Bcl-2 in ATOX1-overexpressing HCC cells. Conversely, opposite trends were observed in HCC cells transfected with siRNA targeting ATOX1 (Fig. 6D and E). We also observed a reduction in apoptotic cell proportions after ATOX1 overexpression and increased apoptosis upon ATOX1 knockdown (Fig. 6F and G). Furthermore, treatment with the ROS inhibitor acetylcysteine reversed the decrease in c-Myb expression induced by ATOX1 knockdown compared to siRNA-ATOX1 treatment alone (Fig. 6H). These results indicated that ATOX1 reduced copper accumulation and ROS production, subsequently affecting c-Myb expression and the PI3K/AKT signaling pathway axis.

Inhibition of ATOX1 reduced cell proliferation and induced ROS production and apoptosis

The organic small molecule DCAC50 has been shown previously to block copper transport chaperones ATOX1 and CCS,

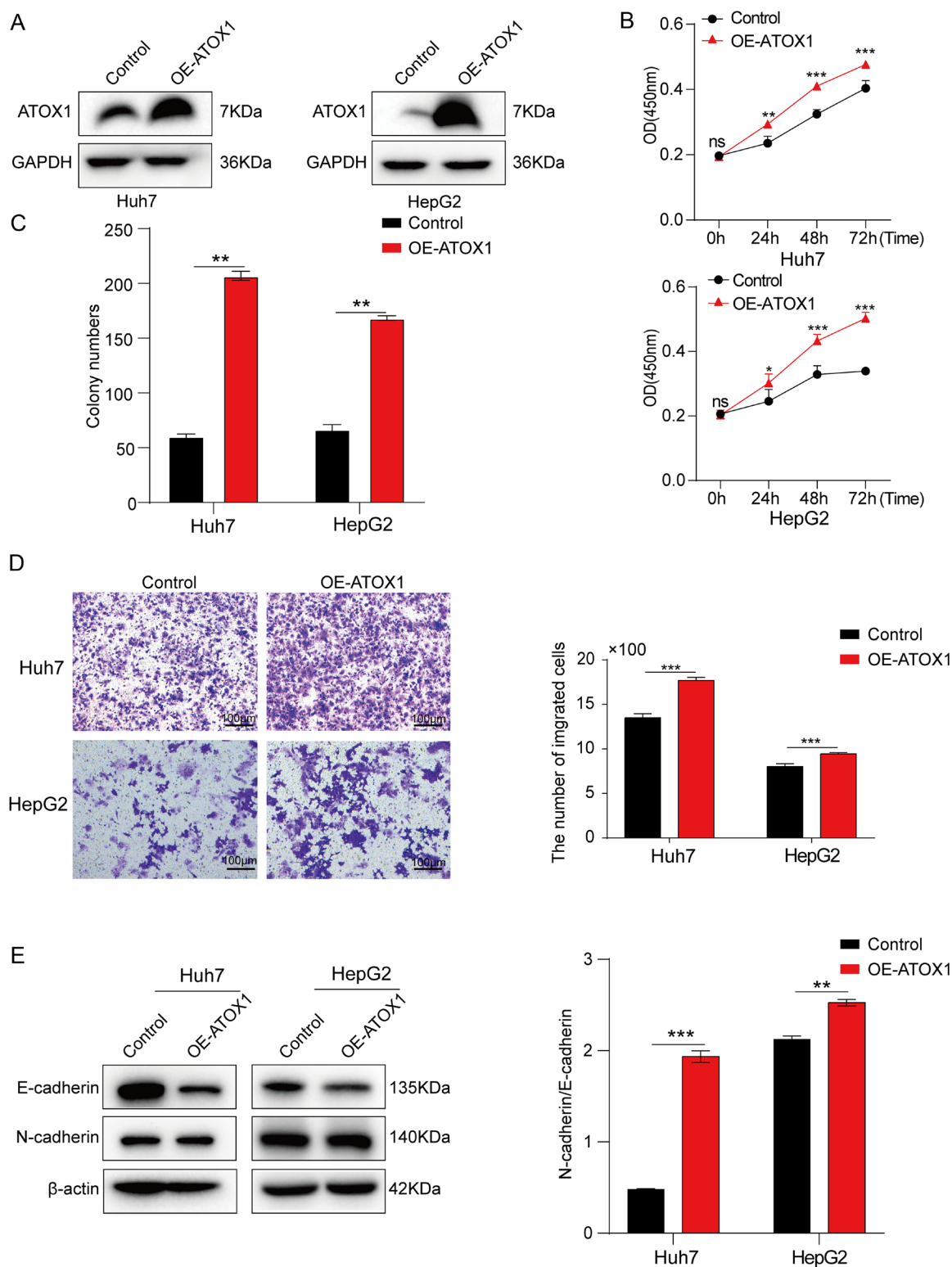


Fig. 2. ATOX1 overexpression affected the proliferation and migration of HCC cells. (A) ATOX1 overexpression was confirmed by Western blot analysis in Huh7 and HepG2 cells. (B) The viability of Huh7 and HepG2 cells overexpressing ATOX1 was evaluated using the CCK-8 assay. (C) The number of colonies in cells overexpressing ATOX1 was assessed by the colony formation assay. (D) Cell migration in Huh7 and HepG2 cells post-ATOX1 overexpression was examined using the Transwell assay. Bar graphs depict the number of cells that migrated to the lower chambers (scale bar, 100 µm; magnification, ×10). (E) The protein expression levels of E-cadherin and N-cadherin were analyzed in Huh7 and HepG2 cells transfected with control or OE-ATOX1 plasmids. The histogram shows a relative quantitative analysis. * $p < 0.05$, ** $p < 0.01$, *** $p < 0.001$. HCC, hepatocellular carcinoma; CCK-8, Cell Counting Kit-8; OE-ATOX1, ATOX1 overexpression; ATOX1, antioxidant-1.

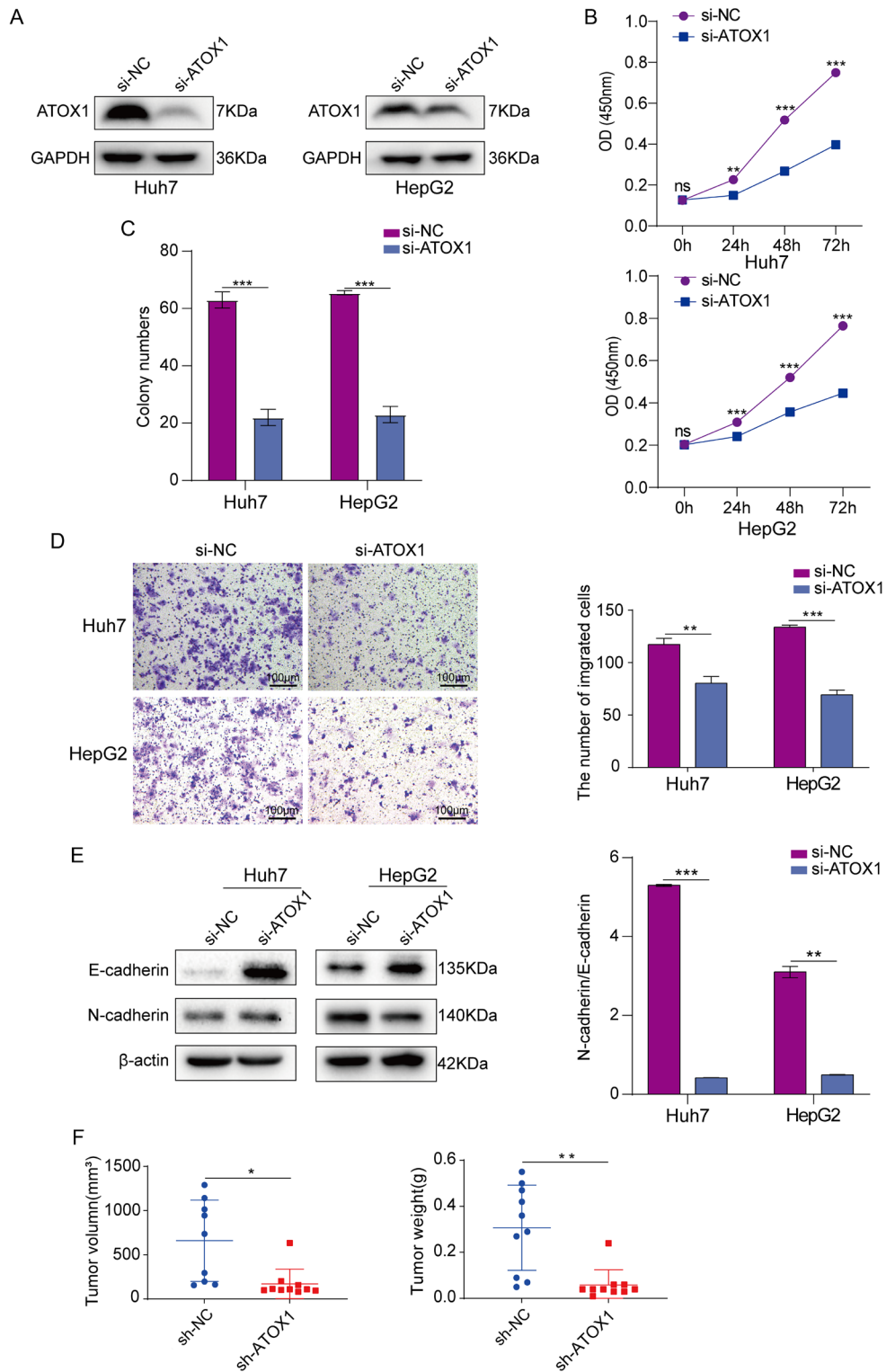


Fig. 3. ATOX1 knockdown affected the proliferation and migration of HCC cells *in vitro* and tumor growth *in vivo*. (A) ATOX1 knockdown was confirmed by Western blot analysis in Huh7 and HepG2 cells. (B and C) The proliferative capacity of Huh7 and HepG2 cells post-ATOX1 knockdown was evaluated by the CCK-8 (B) and colony formation (C) assays. (D) The Transwell assay was performed to assess the migratory ability of Huh7 and HepG2 cells with ATOX1 knockdown (scale bar, 100 μm; magnification, ×10). (E) The protein expression of E-cadherin and N-cadherin was analyzed in Huh7 and HepG2 cells transfected with siRNA-NC or siRNA-ATOX1. (F) After subcutaneous injection of Hep3B^{sh-NC} or Hep3B^{sh-ATOX1} cells in BALB/c nude mice for four weeks, tumor volume and weight were measured. * $p < 0.05$, ** $p < 0.01$, *** $p < 0.001$. HCC, hepatocellular carcinoma; CCK-8, Cell Counting Kit-8; si-NC, small interfering RNA targeting negative control; si-ATOX1, small interfering RNA targeting ATOX1; ATOX1, antioxidant-1.

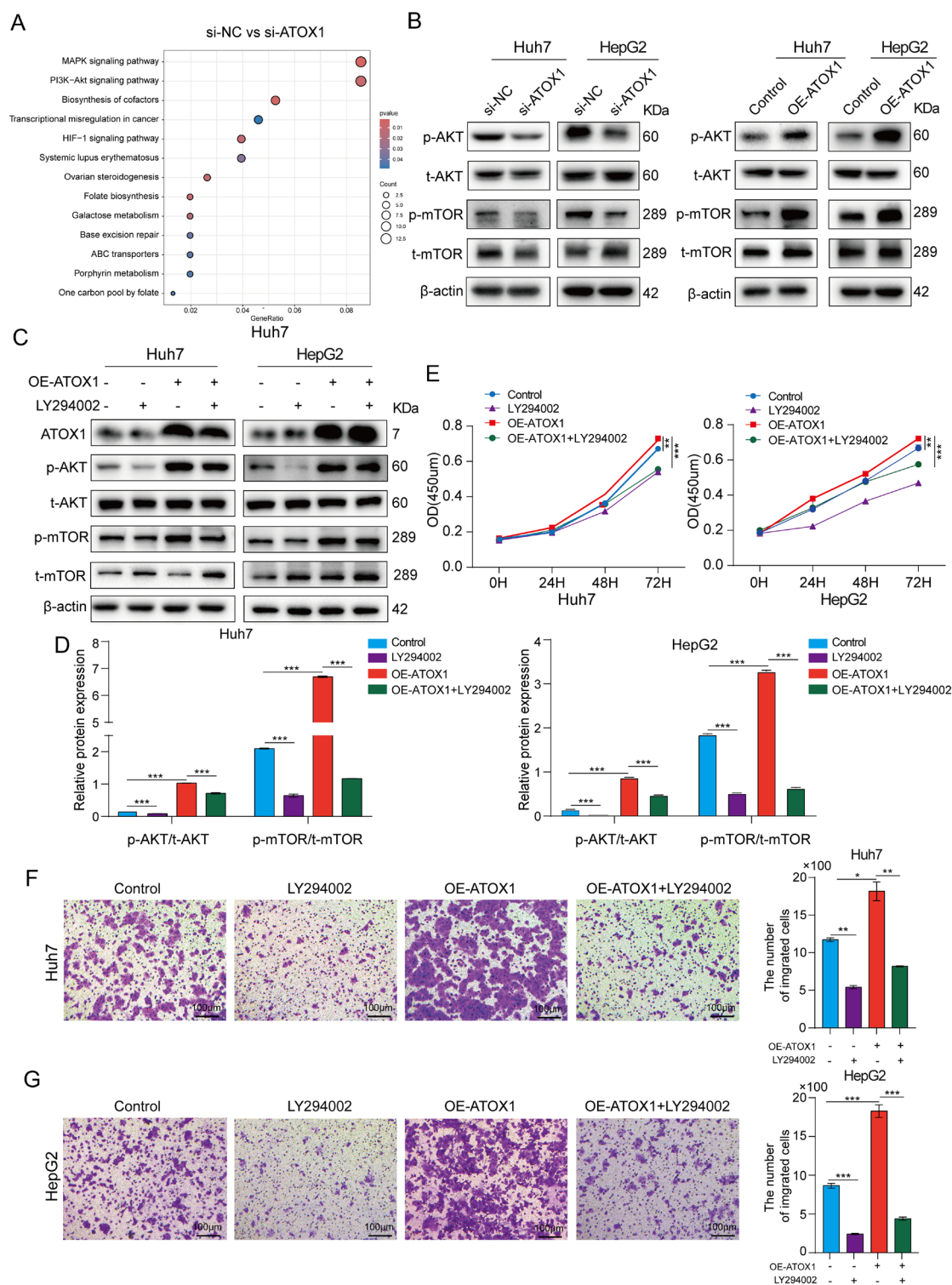


Fig. 4. The impact of ATOX1 on the PI3K/AKT signaling pathway. (A) Enriched pathways through KEGG analysis in the ATOX1 knockdown group. (B) Western blot analysis of phosphorylation levels of AKT and mTOR in HCC cells with ATOX1 knockdown or overexpression. (C and D) Phosphorylation levels of AKT and mTOR in Huh7 and HepG2 cells transfected with the OE-ATOX1 plasmid for 24 h before treatment with LY294002 (20 μM) for 24 h were determined by Western blot (C). The histogram shows a relative quantitative analysis (D). (E) The effect of LY294002 on ATOX1 overexpression-induced cell proliferation was assessed using the CCK-8 assay. (F and G) The effect of LY294002 on ATOX1 overexpression-induced cell migration was measured using the Transwell assay (scale bar, 100 μm; original magnification, ×10). Bar graphs depict the number of cells that migrated to the lower chambers. **p* < 0.05, ***p* < 0.01, ****p* < 0.001. KEGG, Kyoto Encyclopedia of Genes and Genomes; HCC, hepatocellular carcinoma; CCK-8, Cell Counting Kit-8; OE-ATOX1, ATOX1 overexpression; si-NC, small interfering RNA targeting negative control; si-ATOX1, small interfering RNA targeting ATOX1; ATOX1, antioxidant-1.

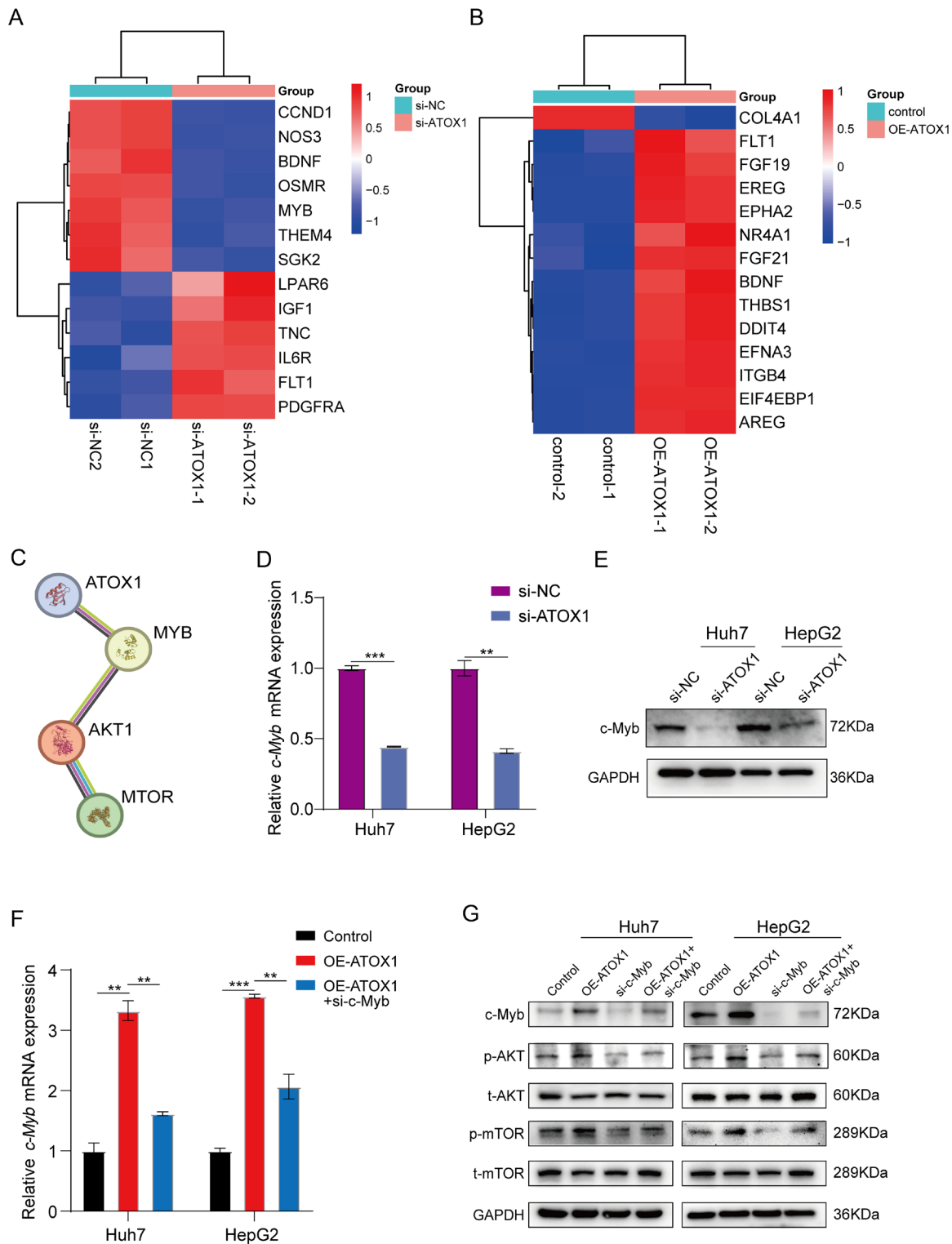


Fig. 5. The role of c-Myb in the impact of ATOX1 on the PI3K/AKT signaling pathway. (A and B) Differential expression of hub genes associated with the PI3K/AKT signaling pathway in groups with ATOX1 knockdown (A) and overexpression (B) revealed by heatmap analysis. (C) PPI network of ATOX1, c-Myb, and the PI3K/AKT pathway was constructed. (D and E) The mRNA (D) and protein (E) expression levels of c-Myb were analyzed in Huh7 and HepG2 cells following ATOX1 knockdown. (F) The mRNA expression of c-Myb was analyzed in HCC cells transfected with the OE-ATOX1 plasmid for 24 h before treatment with siRNA targeting c-Myb for 24 h. (G) The PI3K/AKT pathway was analyzed by Western blot in Huh7 and HepG2 cells transfected with the OE-ATOX1 plasmid for 24 h before treatment with siRNA targeting c-Myb for 24 h. $^{**}p < 0.01$, $^{***}p < 0.001$. PPI, Protein-Protein Interaction Network; HCC, hepatocellular carcinoma; OE-ATOX1, ATOX1 overexpression; si-NC, targeting negative control; si-ATOX1, small interfering RNA targeting ATOX1; si-c-Myb, small interfering RNA targeting c-Myb; ATOX1, antioxidant-1.

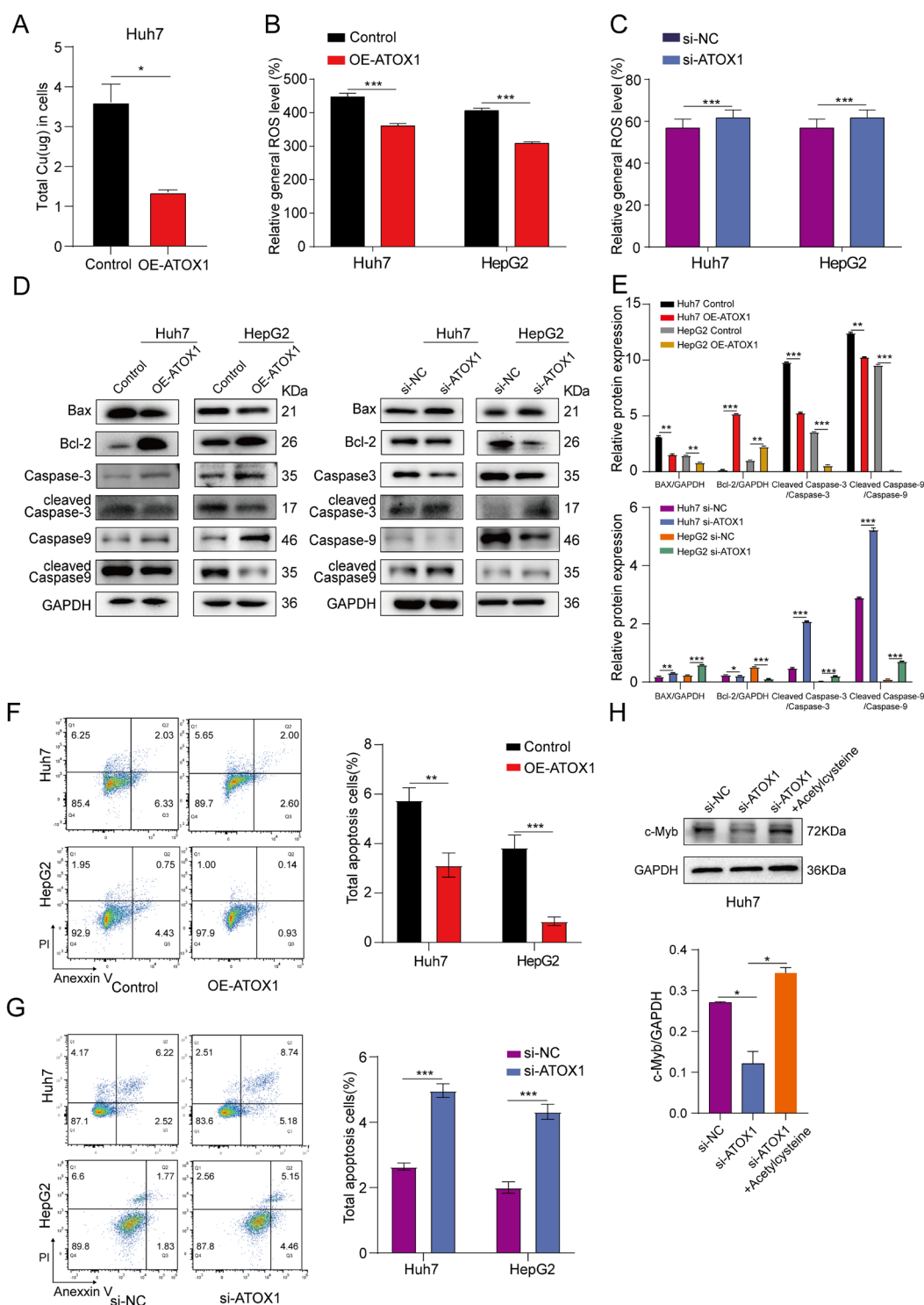


Fig. 6. ATOX1 affected copper accumulation, intracellular ROS levels, and apoptosis in HCC cells. (A) Huh7 cells overexpressing ATOX1 were treated with 100 μ M CuSO_4 for 24 h and then cultured in a medium without CuSO_4 for 24 h. The total cellular copper content was quantified using ICP-MS analysis. (B and C) ROS levels in Huh7 and HepG2 cells with ATOX1 overexpression (B) or knockdown (C) were assessed. (D and E) The expression levels of apoptosis-related proteins, including cleaved Caspase-3, cleaved Caspase-9, BAX, and Bcl-2, were analyzed via Western blot analysis in HCC cells with ATOX1 overexpression or knockdown (D). The histogram shows a relative quantitative analysis (E). (F and G) Annexin V/PI double staining was performed to assess apoptosis in HCC cells. Bar graphs illustrate the quantitative analysis. (H) The protein expression of c-Myb in Huh7 cells transfected with siRNA targeting ATOX1 before treatment with acetylcysteine for 24 h. The histogram shows a relative quantitative analysis. * $p < 0.05$, ** $p < 0.01$, *** $p < 0.001$. HCC, hepatocellular carcinoma; ICP-MS, inductively coupled plasma mass spectrometry; ROS, reactive oxygen species; PI, propidium iodide; OE-ATOX1, ATOX1 overexpression; si-NC, small interfering RNA targeting negative control; si-ATOX1, small interfering RNA targeting ATOX1; ATOX1, antioxidant-1.

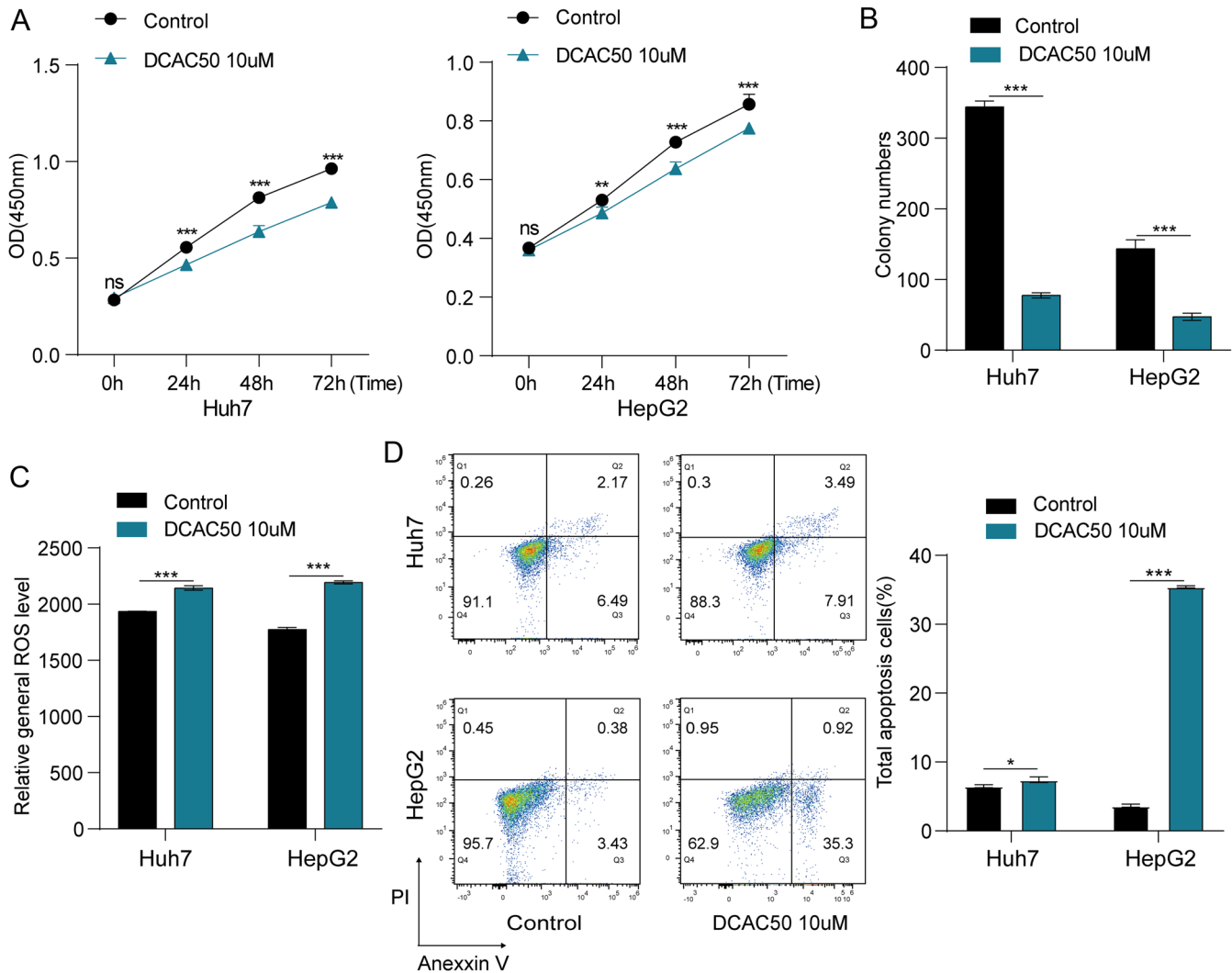


Fig. 7. DCAC50 affected proliferation, intracellular ROS levels, and apoptosis in HCC cells. (A) The viability of HCC cells treated with DCAC50 was analyzed by the CCK-8 assay. (B) The colony-forming ability of HCC cells treated with DCAC50 was examined via the colony formation assay. (C) ROS accumulation in HCC cells treated with DCAC50 was quantified. (D) The effect of DCAC50 on cell apoptosis was analyzed by flow cytometry. Bar graphs present quantitative analysis. * $p < 0.05$, ** $p < 0.01$, *** $p < 0.001$. HCC, hepatocellular carcinoma; CCK-8, Cell Counting Kit-8; ROS, reactive oxygen species; PI, propidium iodide; ATOX1, antioxidant-1.

reducing cell proliferation and elevating oxidative stress and apoptosis in triple-negative breast cancer cells.¹⁴ In line with effects observed following ATOX1 knockdown, treatment with 10 μ M DCAC50 inhibited cell proliferation and colony-forming ability (Fig. 7A and B). We then examined whether ATOX1 inhibition increased cellular ROS levels. As shown in Figure 7C, DCAC50 treatment significantly induced ROS accumulation. Additionally, DCAC50 increased cell apoptosis (Fig. 7D). These data indicated that DCAC50-mediated inhibition of ATOX1 suppressed proliferation while promoting ROS accumulation and apoptosis in Huh7 and HepG2 cells.

Discussion

Understanding the underlying molecular mechanisms involved in HCC carcinogenesis is essential for developing effective treatment strategies for HCC patients. Previous studies have demonstrated that the upregulation of the copper

transporter protein ATOX1 is closely associated with various cancers and plays a significant role in tumorigenesis through complex mechanisms.^{12–17} ATOX1 is notably expressed in liver tissue, a primary site of copper metabolism. However, to our knowledge, the mechanisms by which ATOX1 contributes to HCC remain largely unknown. In this study, we found that ATOX1 may promote HCC carcinogenesis through activation of the c-Myb/PI3K/AKT pathway, accompanied by inhibition of copper accumulation, oxidative stress generation, and apoptosis (Graphical abstract).

Our analysis explored the role of ATOX1 in HCC tumorigenicity. Functional experiments demonstrated that ATOX1 promotes proliferation, colony formation, and migration of HCC cells. *In vivo*, ATOX1 knockdown inhibited the growth of subcutaneous tumors in nude mice. Moreover, ATOX1 expression was upregulated in HCC tissues compared to normal liver tissues. Consequently, investigating the mechanisms underlying ATOX1 upregulation in HCC is imperative.

To explore the mechanisms by which ATOX1 exerts its

oncogenic effects, we conducted KEGG enrichment analyses on RNA-sequencing data. DEGs in cells with ATOX1 overexpression and knockdown were associated with the PI3K/AKT signaling pathway. This pathway is a critical signaling cascade in malignant tumors, promoting proliferation, metastasis, and angiogenesis.³⁰ It is upregulated in 40%–50% of HCC cases, with aberrant activation linked to poor tumor differentiation, prognosis, and early recurrence.³¹ Bioactive PI3K catalyzes the conversion of PIP2 to PIP3, subsequently recruiting the key downstream protein AKT. Activated AKT then targets downstream molecules, with mTOR being a prominent effector.³² Our findings indicated that phosphorylation of AKT and mTOR was reduced after ATOX1 knockdown, whereas ATOX1 overexpression increased AKT and mTOR phosphorylation. The inhibition of PI3K signaling via LY294002 markedly reduced ATOX1-induced activation of the PI3K/AKT pathway and suppressed proliferation and migration of ATOX1-transfected cells. These results suggested that ATOX1 might function as an oncogenic factor in HCC cells by activating the PI3K/AKT signaling pathway.

Furthermore, RNA sequencing of cells with ATOX1 overexpression and knockdown identified c-Myb as a gene related to the PI3K/AKT signaling pathway and potentially associated with ATOX1 (Supplementary Fig. 5). MYB transcription factors, including c-MYB, A-MYB, and B-MYB, are implicated in cell proliferation, survival, and differentiation.³³ c-Myb is known to regulate cell proliferation, invasion, and apoptosis and is linked to the activation of the Erk and PI3K/AKT signaling pathways.^{27,28,34} Therefore, we hypothesized that ATOX1 might upregulate c-Myb to activate the PI3K/AKT signaling pathway. Although IP analysis in Huh7 and HepG2 cells revealed no direct interaction between ATOX1 and c-Myb, our findings demonstrated that ATOX1 upregulates c-Myb at both the mRNA and protein levels and activates AKT and mTOR phosphorylation through c-Myb upregulation. This implied that ATOX1 may enhance c-Myb expression at the transcriptional level; however, further evidence, such as dual luciferase reporter assays and chromatin immunoprecipitation, is needed to clarify how ATOX1 modulates c-Myb transcriptional activity.

Copper is a redox-active transition metal integral to mitochondrial respiration, angiogenesis, antioxidant defense, and redox signaling. Intracellular free copper homeostasis is meticulously regulated by a complex system of copper transporters and chaperone proteins to prevent copper overload.^{35,36} Excessive intracellular copper accumulation or alterations in its redistribution can lead to increased ROS generation. Oxidative stress arises from an imbalance between ROS and antioxidants. Elevated ROS levels are associated with various pathologies, including aging, inflammation, neurodegenerative diseases, atherosclerosis, and cancer.³⁷ Therefore, to maintain intracellular ROS homeostasis, early-stage cancer cells must regulate ROS within a specific threshold, which also depends on the antioxidant defense system.^{38,39} We postulated that the oncogenic effects of ATOX1 are linked to its copper transport function. The ICP-MS assay demonstrated a marked reduction in total intracellular copper levels in Huh7 cells overexpressing ATOX1 when cultured in the medium supplemented with 100 μ M CuSO₄, a concentration that did not significantly affect cell viability. Additionally, cell death induced by excessive copper, termed cuproptosis, may contribute to the pathogenesis of various cancers. Interestingly, a recent study identified an association between ATOX1 and cuproptosis via differential gene expression analysis.⁴⁰ Subsequent research confirmed that the cuproptosis-related gene LIPT1 suppresses the progression of non-small cell lung cancer by targeting ATOX1.⁴¹ ATOX1 is hypothesized to function as a copper chaperone protein, potentially promoting HCC

progression by regulating copper ion transport. However, its precise role in the mechanism of cuproptosis remains unclear and warrants further investigation.

ATOX1 was initially identified in yeast as an antioxidant enzyme that protects cells from scavenging damage and hydrogen peroxide (H₂O₂) toxicity.⁴² It plays a crucial role in antioxidant defense and is upregulated in various cancers. Kim *et al.* demonstrated that the transduction of Tat-ATOX1 protein in hippocampal HT-22 cells protects against oxidative stress, offering therapeutic potential for transient forebrain ischemia and other oxidative stress-related neuronal diseases.⁴³ Jeney *et al.* discovered that ATOX1 functions as a copper chaperone for superoxide dismutase 3 and positively regulates its transcription, thereby modulating oxidative stress in the cardiovascular system.⁴⁴ Inhibition of ATOX1 and CCS by small molecules leads to elevated copper levels and ROS accumulation, inducing apoptosis and reducing cell proliferation in various cancers, including lung, leukemia, breast, head, and neck cancers.^{14,15,45} Consistent with these reports, we observed a significant reduction in ROS production in HCC cells overexpressing ATOX1, whereas ATOX1 knockdown increased ROS levels. Moreover, ATOX1 overexpression reduced the number of apoptotic cells and decreased the expression of apoptosis-related proteins, while ATOX1 knockdown promoted apoptosis. Similarly, disruption of ATOX1's copper transport function via DCAC50 inhibited the proliferation of HCC cells and increased ROS generation and apoptosis. Notably, acetylcysteine, a ROS inhibitor, reversed the decrease in c-Myb expression induced by ATOX1 knockdown. These findings support the hypothesis that ATOX1 promotes HCC carcinogenicity by reducing copper accumulation and ROS toxicity, thereby modulating c-Myb expression and the PI3K/AKT signaling pathway.

Analysis of TCGA data via the UALCAN website and immunohistochemical examination of HCC tissues revealed elevated ATOX1 expression in tumor tissues. However, no significant correlation was found between ATOX1 expression and HCC malignancy or prognosis, possibly due to small sample size or cohort heterogeneity. Nonetheless, given ATOX1's potential role in HCC carcinogenesis, it may serve as a valuable molecular biomarker for patients with HCC. Further studies in larger, well-organized cohorts are needed to clarify the clinical relevance and mechanisms of ATOX1 in HCC.

Conclusions

This study elucidates that ATOX1 promotes HCC carcinogenicity through the c-Myb/PI3K/AKT signaling pathway while inhibiting copper accumulation, ROS generation, and apoptosis. These results indicate that ATOX1 represents a potential therapeutic target for HCC. Moreover, the compound DCAC50, by obstructing ATOX1's copper transport function, effectively suppresses the malignant behavior of HCC cells, suggesting its promising role in HCC treatment, particularly when combined with PI3K/AKT pathway inhibitors.

Funding

This study was supported by grants from the Nature Science Foundation of China (no. 81650014) and Digestive Medical Coordinated Development Center of Beijing Municipal Administration of Hospitals (no. XXZ0501, XXX0101, XXT03).

Conflict of interest

The authors have no conflict of interests related to this publication.

Author contributions

Conceptualizing and/or supervising the study: JH and DZ; Performing the most experiments and analyzing and interpreted the data: QO and SJ; Providing technical support: YmL, DZ, and AX. Participating in consumable reagent support: HT and YL; Engaged in animal experiments: QZ, HZ, SC; Providing clinical analysis and professional assessment: PH. XW and XO; Manuscript written: QY; Manuscript revision: JH and DZ. All authors have read and approved the final version and publication of the manuscript.

Ethical statement

The study protocols were performed in accordance with the Declaration of Helsinki as revised in 2024, and approved by the Clinical Research Ethics Committee of Beijing Friendship Hospital, Capital Medical University (Number 2023-P2-006-01), and the Animal Experiments and Experimental Animal Welfare Committee of Beijing Friendship Hospital, Capital Medical University (Number 22-2023). Written informed consent was obtained from all participants.

Data sharing statement

The datasets generated during and/or analyzed during the current study are available from the corresponding author on reasonable request.

References

- Bray F, Laversanne M, Sung H, Ferlay J, Siegel RL, Soerjomataram I, *et al*. Global cancer statistics 2022: GLOBOCAN estimates of incidence and mortality worldwide for 36 cancers in 185 countries. *CA Cancer J Clin* 2024;74(3):229–263. doi:10.3322/caac.21834, PMID:38572751.
- Li L, Li ZZ, Pan LX, Su JY, Huang S, Ma L, *et al*. Adjuvant Therapy for Hepatocellular Carcinoma After Curative Treatment: Several Unanswered Questions. *J Clin Transl Hepatol* 2024;12(5):525–533. doi:10.14218/JCTH.2024.00030, PMID:38779519.
- Gordan JB, Kennedy EB, Abou-Alfa GK, Beal E, Finn RS, Gade TP, *et al*. Systemic Therapy for Advanced Hepatocellular Carcinoma: ASCO Guideline Update. *J Clin Oncol* 2024;42(15):1830–1850. doi:10.1200/JCO.23.02745, PMID:38502889.
- Vitaliti A, De Luca A, Rossi L. Copper-Dependent Kinases and Their Role in Cancer Inception, Progression and Metastasis. *Biomolecules* 2022;12(10):1520. doi:10.3390/biom12101520, PMID:36291728.
- Ackerman CM, Chang CJ. Copper signaling in the brain and beyond. *J Biol Chem* 2018;293(13):4628–4635. doi:10.1074/jbc.R117.000176, PMID:29084848.
- Denoyer D, Masaldan S, La Fontaine S, Cater MA. Targeting copper in cancer therapy: 'Copper That Cancer'. *Metallomics* 2015;7(11):1459–1476. doi:10.1039/c5mt00149h, PMID:26313539.
- Gupte A, Mumper RJ. Elevated copper and oxidative stress in cancer cells as a target for cancer treatment. *Cancer Treat Rev* 2009;35(1):32–46. doi:10.1016/j.ctrv.2008.07.004, PMID:18774652.
- Hayes JD, Dinkova-Kostova AT, Tew KD. Oxidative Stress in Cancer. *Cancer Cell* 2020;38(2):167–197. doi:10.1016/j.ccell.2020.06.001, PMID:32649885.
- Vo TTT, Peng TY, Nguyen TH, Bui TNH, Wang CS, Lee WJ, *et al*. The cross-talk between copper-induced oxidative stress and cuproptosis: a novel potential anticancer paradigm. *Cell Commun Signal* 2024;22(1):353. doi:10.1186/s12964-024-01726-3, PMID:38970072.
- Hatori Y, Lutsenko S. The Role of Copper Chaperone Atox1 in Coupling Redox Homeostasis to Intracellular Copper Distribution. *Antioxidants (Basel)* 2016;5(3):25. doi:10.3390/antiox5030025, PMID:27472369.
- Hatori Y, Lutsenko S. An expanding range of functions for the copper chaperone/antioxidant protein Atox1. *Antioxid Redox Signal* 2013;19(9):945–957. doi:10.1089/ars.2012.5086, PMID:23249252.
- Chen L, Li N, Zhang M, Sun M, Bian J, Yang B, *et al*. APEX2-based Proximity Labeling of Atox1 Identifies CRIP2 as a Nuclear Copper-binding Protein that Regulates Autophagy Activation. *Angew Chem Int Ed Engl* 2021;60(48):25346–25355. doi:10.1002/anie.202108961, PMID:34550632.
- Itoh S, Kim HW, Nakagawa O, Ozumi K, Lessner SM, Aoki H, *et al*. Novel role of antioxidant-1 (Atox1) as a copper-dependent transcription factor involved in cell proliferation. *J Biol Chem* 2008;283(14):9157–9167. doi:10.1074/jbc.M709463200, PMID:18245776.
- Wang J, Luo C, Shan C, You Q, Lu J, Elf S, *et al*. Inhibition of human copper trafficking by a small molecule significantly attenuates cancer cell proliferation. *Nat Chem* 2015;7(12):968–979. doi:10.1038/nchem.2381, PMID:26587712.
- Karginova O, Weekley CM, Raoul A, Alsayed A, Wu T, Lee SS, *et al*. Inhibition of Copper Transport Induces Apoptosis in Triple-Negative Breast Cancer Cells and Suppresses Tumor Angiogenesis. *Mol Cancer Ther* 2019;18(5):873–885. doi:10.1158/1535-7163.MCT-18-0667, PMID:30824611.
- Jana A, Das A, Krett NL, Guzman G, Thomas A, Mancinelli G, *et al*. Nuclear translocation of Atox1 potentiates activin A-induced cell migration and colony formation in colon cancer. *PLoS One* 2020;15(1):e0227916. doi:10.1371/journal.pone.0227916, PMID:31961892.
- Blockhuys S, Zhang X, Wittung-Stafshede P. Single-cell tracking demonstrates copper chaperone Atox1 to be required for breast cancer cell migration. *Proc Natl Acad Sci U S A* 2020;117(4):2014–2019. doi:10.1073/pnas.1910722117, PMID:31932435.
- Li Y, Ouyang Q, Chen Z, Zhou D, Li Z, Yang X, *et al*. Novel role of general transcript factor ITH subunit 2 (GTF2H2) in the development and sex disparity of hepatocellular carcinoma. *Oncogene* 2025;44(19):1323–1335. doi:10.1038/s41388-025-03301-7, PMID:39972070.
- Yin J, Shao Y, Huang F, Hong Y, Wei W, Jiang C, *et al*. Peroxisomal membrane protein PMP70 confers drug resistance in colorectal cancer. *Cell Death Dis* 2025;16(1):293. doi:10.1038/s41419-025-07572-6, PMID:40229252.
- Xu Y, Zhou W, Ji Y, Shen J, Zhu X, Yu H, *et al*. Elongator promotes the migration and invasion of hepatocellular carcinoma cell by the phosphorylation of AKT. *Int J Biol Sci* 2018;14(5):518–530. doi:10.7150/ijbs.23511, PMID:29805303.
- Ouyang Q, Li Y, Xu A, Zhang N, Chen S, Zhou D, *et al*. Recurrent BMP4 variants in exon 4 cause non-HFE-associated hemochromatosis via the BMP/SMAD signaling pathway. *Orphanet J Rare Dis* 2024;19(1):429. doi:10.1186/s13023-024-03439-9, PMID:39563390.
- Paul S, Patra D, Kundu R. Lignan enriched fraction (LRF) of *Phyllanthus amarus* promotes apoptotic cell death in human cervical cancer cells in vitro. *Sci Rep* 2019;9(1):14950. doi:10.1038/s41598-019-51480-7, PMID:31628385.
- Zhao Y, Tang J, Yang D, Tang C, Chen J. Staphylococcal enterotoxin M induced inflammation and impairment of bovine mammary epithelial cells. *J Dairy Sci* 2020;103(9):8350–8359. doi:10.3168/jds.2019-17444, PMID:32622596.
- Zhou C, Yi C, Yi Y, Qin W, Yan Y, Dong X, *et al*. LncRNA PVT1 promotes gemcitabine resistance of pancreatic cancer via activating Wnt/ β -catenin and autophagy pathway through modulating the miR-619-5p/Pygo2 and miR-619-5p/ATG14 axes. *Mol Cancer* 2020;19(1):118. doi:10.1186/s12943-020-01237-y, PMID:32727463.
- Sun EJ, Wankell M, Palamuthusingam P, McFarlane C, Hebbard L. Targeting the PI3K/Akt/mTOR Pathway in Hepatocellular Carcinoma. *Biomedicines* 2021;9(11):1639. doi:10.3390/biomedicines9111639, PMID:34829868.
- Tan Y, Cheng H, Su C, Chen P, Yang X. PI3K/Akt Signaling Pathway Ameliorates Oxidative Stress-Induced Apoptosis upon Manganese Exposure in PC12 Cells. *Biol Trace Elem Res* 2022;200(2):749–760. doi:10.1007/s12011-021-02687-1, PMID:33772736.
- Bu C, Xu L, Han Y, Wang M, Wang X, Liu W, *et al*. c-Myb protects cochlear hair cells from cisplatin-induced damage via the PI3K/Akt signaling pathway. *Cell Death Discov* 2022;8(1):78. doi:10.1038/s41420-022-00879-9, PMID:35210433.
- Zhang J, Shu Y, Qu Y, Zhang L, Chu T, Zheng Y, *et al*. C-myb Plays an Essential Role in the Protective Function of IGF-1 on Cytotoxicity Induced by A β (25–35) via the PI3K/Akt Pathway. *J Mol Neurosci* 2017;63(3–4):412–418. doi:10.1007/s12031-017-0991-0, PMID:29110181.
- Zubair H, Patel GK, Khan MA, Azim S, Zubair A, Singh S, *et al*. Proteomic Analysis of MYB-Regulated Secretome Identifies Functional Pathways and Biomarkers: Potential Pathobiological and Clinical Implications. *J Proteome Res* 2020;19(2):794–804. doi:10.1021/acs.jproteome.9b00641, PMID:31928012.
- Glaviano A, Foo ASC, Lam HY, Yap KCH, Jacot W, Jones RH, *et al*. PI3K/AKT/mTOR signaling transduction pathway and targeted therapies in cancer. *Mol Cancer* 2023;22(1):138. doi:10.1186/s12943-023-01827-6, PMID:37596643.
- Matter MS, Decaens T, Andersen JB, Thorgeirsson SS. Targeting the mTOR pathway in hepatocellular carcinoma: current state and future trends. *J Hepatol* 2014;60(4):855–865. doi:10.1016/j.jhep.2013.11.031, PMID:24308993.
- He Y, Sun MM, Zhang GG, Yang J, Chen KS, Xu WW, *et al*. Targeting PI3K/Akt signal transduction for cancer therapy. *Signal Transduct Target Ther* 2021;6(1):425. doi:10.1038/s41392-021-00828-5, PMID:34916492.
- Cicirò Y, Sala A. MYB oncoproteins: emerging players and potential therapeutic targets in human cancer. *Oncogenesis* 2021;10(2):19. doi:10.1038/s41389-021-00309-y, PMID:33637673.
- Anand S, Vikramdeo KS, Sudan SK, Sharma A, Acharya S, Khan MA, *et al*. From modulation of cellular plasticity to potentiation of therapeutic resistance: new and emerging roles of MYB transcription factors in human malignancies. *Cancer Metastasis Rev* 2024;43(1):409–421. doi:10.1007/s10555-023-10153-8, PMID:37950087.
- Jiang Y, Huo Z, Qi X, Zuo T, Wu Z. Copper-induced tumor cell death mechanisms and antitumor therapeutic applications of copper complexes. *Nanomedicine (Lond)* 2022;17(5):303–324. doi:10.2217/nnm-2021-0374, PMID:35060391.
- Gaetke LM, Chow-Johnson HS, Chow CK. Copper: toxicological relevance and mechanisms. *Arch Toxicol* 2014;88(11):1929–1938. doi:10.1007/s00204-014-1355-y, PMID:25199685.
- Brieger K, Schiavone S, Miller FJ Jr, Krause KH. Reactive oxygen species: from health to disease. *Swiss Med Wkly* 2012;142:w13659. doi:10.4414/smw.2012.13659, PMID:22903797.
- Prasad S, Gupta SC, Tyagi AK. Reactive oxygen species (ROS) and can-

- cer: Role of antioxidative nutraceuticals. *Cancer Lett* 2017;387:95–105. doi:10.1016/j.canlet.2016.03.042, PMID:27037062.
- [39] Zhang Y, Xu Y, Lu W, Ghergurovich JM, Guo L, Blair IA, *et al*. Upregulation of Antioxidant Capacity and Nucleotide Precursor Availability Sufices for Oncogenic Transformation. *Cell Metab* 2021;33(1):94–109.e8. doi:10.1016/j.cmet.2020.10.002, PMID:33159852.
- [40] Zou M, Zhang W, Zhu Y, Xu Y. Identification of 6 cuproptosis-related genes for active ulcerative colitis with both diagnostic and therapeutic values. *Medicine (Baltimore)* 2023;102(43):e35503. doi:10.1097/MD.00000000000035503, PMID:37904461.
- [41] Deng R, Zhu L, Jiang J, Chen J, Li H. Cuproptosis-related gene LIPT1 as a prognostic indicator in non-small cell lung cancer: Functional involvement and regulation of ATOX1 expression. *Biomol Biomed* 2024;24(3):647–658. doi:10.17305/bb.2023.9931, PMID:38041690.
- [42] Lin SJ, Culotta VC. The ATX1 gene of *Saccharomyces cerevisiae* encodes a small metal homeostasis factor that protects cells against reactive oxygen toxicity. *Proc Natl Acad Sci U S A* 1995;92(9):3784–3788. doi:10.1073/pnas.92.9.3784, PMID:7731983.
- [43] Kim SM, Hwang IK, Yoo DY, Eum WS, Kim DW, Shin MJ, *et al*. Tat-antioxidant 1 protects against stress-induced hippocampal HT-22 cells death and attenuate ischaemic insult in animal model. *J Cell Mol Med* 2015;19(6):1333–1345. doi:10.1111/jcmm.12513, PMID:25781353.
- [44] Jeney V, Itoh S, Wendt M, Gradek Q, Ushio-Fukai M, Harrison DG, *et al*. Role of antioxidant-1 in extracellular superoxide dismutase function and expression. *Circ Res* 2005;96(7):723–729. doi:10.1161/01.RES.0000162001.57896.66, PMID:15761197.
- [45] Ding F, Li F, Tang D, Wang B, Liu J, Mao X, *et al*. Restoration of the Immunogenicity of Tumor Cells for Enhanced Cancer Therapy via Nanoparticle-Mediated Copper Chaperone Inhibition. *Angew Chem Int Ed Engl* 2022;61(31):e202203546. doi:10.1002/anie.202203546, PMID:35642869.